Asian Journal of Chemistry; Vol. 34, No. 1 (2022), 223-229

ASIAN JOURNAL OF CHEMISTRY

https://doi.org/10.14233/ajchem.2022.23485

Synthesis, Characterization, Semiconductor-Assisted Photocatalysis and Antibacterial Activity of Electrochemically Synthesized SnS and NiS/SnS Nano Photocatalysts

HOSAHOLALU BALAKRISHNA UMA[1], MALAHALLI S. VIJAYA KUMAR[1,2,*] and SANNAIAH ANANDA[1]

[1]Department of Studies in Chemistry, University of Mysore, Manasagangotri, Mysuru-570006, India
[2]Vijnana Bhavana, University of Mysore, Manasagangotri, Mysuru-570006, India

*Corresponding author: E-mail: vijayakumar@chemistry.uni-mysore.ac.in

Received: 17 August 2021; *Accepted*: 11 October 2021; *Published online*: 16 December 2021; AJC-20639

In present study, SnS and NiS/SnS nano-photocatalysts have been synthesized by simple electrochemical method and their photocatalytic activity and bacterial inactivation were investigated. The size, morphology, chemical composition and optical properties were investigated by X-ray diffraction (XRD), scanning electron microscope (SEM), energy dispersive X-ray analysis (EDAX) and optical absorption spectroscopy. The XRD analysis confirmed the crystalline SnS phase. The band gap estimated from Tauc's plot was 2.9 eV for SnS and 2.7 eV for NiS/SnS nanoparticles shows that they are photoactive under UV light radiation. The photocatalytic activity of nanoparticles was studied by degradation of textile dye Indigo carmine under ultraviolet radiation and the photocatalytic decolourization of the dye follows the first order kinetics. The antibacterial susceptibility of SnS and NiS/SnS nanoparticles was evaluated by disc diffusion Kirby-Bauer method using *Staphylococcus aureus* and *Escherichia coli.*

Keywords: Stannous sulphide, NiS/SnS, Electrochemical synthesis, Photocatalysis.

INTRODUCTION

In recent years, considerable interest has been shown on semiconducting nanostructures owing to their enhanced electrical and optical properties due to the quantum confinement effect [1]. The nanostructures of germanium sulphide (GeS), stannous sulphide (SnS) and lead sulphide (PbS) are important materials among the IV-VI group semiconductors. Studies on stannous sulfide (SnS) gained more interest due to its less toxic nature and layer property compared to other similar materials such as cadmium and lead compounds. Tin sulfide (SnS) is a IV-VI semiconductor material, which can be used as the absorber layer in solar cells and has gained importance because of its attractive optoelectronic properties, non-toxicity and the abundance of constituent elements Sn and S [2,3]. In addition to solar cells, the potential applications of this material include photocatalysis, optoelectronic devices, near IR detector and anode material in lithium ion batteries [4-7].

Tin sulphide (Sn-S) nanostructures have been synthesized by various methods such as hydrothermal, solvothermal, electron beam evaporation and wet chemical route among others [8-11]. The properties of SnS thin films have been investigated by many researchers prepared by various methods such as chemical deposition, electrochemical deposition, electron beam evaporation, thermal evaporation technique, spray pyrolytic deposition, plasma enhanced chemical vapour deposition and chemical bath deposition and radio frequency sputtering [12-19]. Thin films of SnS have attracted much attention because of their potential applications in solar cells, photovoltaic and opto-electronic devices [12,20]. Widely different values of direct and indirect band gap in SnS thin films and nanostructures have been reported. An optical band gap in the range of 1.1-1.75 eV for SnS thin films [21,22] and 1.8-3.6 eV for SnS nanoparticles [23,24] has been reported. No work has been reported for SnS and Ni doped SnS nanoparticles synthesized by electrochemical method.

In present work, we have successfully synthesized SnS and NiS/SnS nanoparticles through a simple, cost effective and eco-friendly electrochemical method. The kinetics of photo catalytic degradation of Indigo carmine dye and antibacterial susceptibility of the synthesized nano-photocatalysts were reported.

EXPERIMENTAL

All chemicals were of analytical grade and used without any further purification. Tin and nickel metal wires from Alfa-asear Pvt Ltd., Platinum electrode from Elico Pvt. Ltd., Sodium sulphide from Alfa asear were used. Deionized water produced from PURELAB ultrawater purification system was used for all the experiments.

Electrochemical synthesis of SnS nanoparticles: SnS nanoparticles were synthesized by electrochemical process using tin and platinum electrodes using sodium sulphide as conductive salt. The electrolytic cell consisted of 0.2 M aqueous Na_2S and electrodes were separated by 1 cm apart. The electrolysis has been carried out for 2 h without stirring using potential difference of 7 V and 12 mA current. During the electrolysis tin electrode acts as anode starts to dissolve and gives Sn^{2+} ions, which were electrochemically reacted with sulphide ions furnished by sodium sulphide to give SnS nanoparticles. The obtained nanoparticles were washed repeatedly with distilled water for complete removal of Na_2S, centrifuged and calcinated at 600 ºC to remove sodium and hydroxide impurities.

Electrochemical synthesis of NiS/SnS nanoparticles: The experimental setup for NiS/SnS was similar to synthesis of SnS (Fig. 1). In this case, Sn and Ni electrodes were used as anode and platinum electrode as cathode. The rate of electrochemical reaction is not same for Sn^{2+} and Ni^{2+} as the redox potentials for Sn^{2+} and Ni^{2+} are different. Since the dissolution potential of Ni (-0.26 eV) is more negative than Sn (-0.14 eV), the formation of NiS takes place in competation with SnS. The mechanism of electrochemical synthesis takes place according to following **Scheme-I**.

$$Sn \rightleftharpoons Sn^{2+} + 2e^-$$
$$Ni \rightleftharpoons Ni^{2+} + 2e^-$$
$$Na_2S \rightleftharpoons 2Na^+ + S^{2-}$$
$$2Na^+ + 2e^- \longrightarrow 2Na \text{ (at Pt e}^-\text{de)}$$
$$Sn^{2+} + S^{2-} \rightleftharpoons SnS$$
$$Ni^{2+} + S^{2-} \rightleftharpoons NiS$$

Scheme-I: Mechanism of electrochemical formation of NiS/SnS nanoparticles

Characterization: FT-IR spectra were recorded using JASCO FT-IR with wave number ranging from 4000-400 cm^{-1}. The SEM images of the sample were recorded on ESEM Quanta 200 FEI-Netherlands scanning electron microscope. The powder X ray diffractions were recorded using Rigaku miniflex II desktop X ray diffractometer (Cu*K*α, λ = 1.54 Å) scan rate of 0.02º/S range from 0º to 60º. The optical absorption spectra have been observed by UV-Vis spectrophotometer at room temperature with JASCO-UV Vis spectrometer.

Mineralization of Indigo carmine dye: The concentration of dye, dopant, pH of the solution, dosage of photocatalyst and exposure to different sources of light *viz*. sunlight and UV light are the variables that influence the photoreactivity of the nanocatalysts [25,26]. To evaluate the photocatalytic efficiency of the prepared nanoparticles, photodegradation experiments were carried out using different concentration of Indigo carmine dye as substrate and different concentrations of SnS and NiS/SnS as catalyst. A calculated quantity of nanoparticles was added to the dye solution, stirred in dark for 1 min to establish adsorption/desorption equilibrium between the dye and nanoparticle molecules and the illuminated under UV source to induce a photochemical reaction. The % T was determined by Elico SL 171 mini spectrometer for aliquots taken at an interval of 10 min. Adsorption and photocatalytic conversion (g%) was calculated. The chemical oxygen demand was measured according to the standard dichromate titration method. The decrease in COD of the solution gives the measure of mineralization of the dye solution.

Antibacterial activity: The antibacterial susceptibility of SnS and NiS/SnS nanoparticles was evaluated by Kirby-Bauer disc diffusion method [27]. Nanoparticles were loaded into 6 mm sterile discs and placed on the culture Gram-positive *Staphylococcus aureus* (MTCC 7443) and Gram-negative *Escherichia coli* (MTCC 40) inoculated Mueller Hinton agar plates and incubated at 37 ºC for 24 h. The comparative stability of discs containing gentamycin was made. The antibacterial susceptibility of synthesized nanoparticles was investigated qualitatively by zone of inhibition. Disposable plates inoculated with the tested Gram-positive and Gram-negative bacteria, such as *Staphylococcus aureus* and *Escherichia coli* at a concentration of 10^5 to 10^6 CFU/mL were used for the tests.

RESULTS AND DISCUSSION

X-ray diffraction studies: It has been reported in the literature that SnS crystallizes in orthorhombic structure, but at higher temperature (> 400 ºC) their crystal structure probably

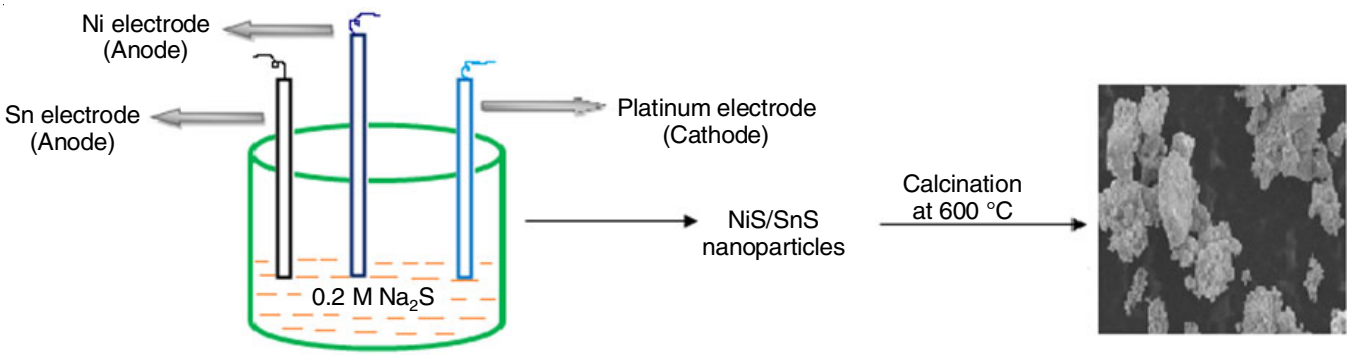

Fig. 1. Diagramatic representation of electrochemical formation of NiS/SnS nanoparticles

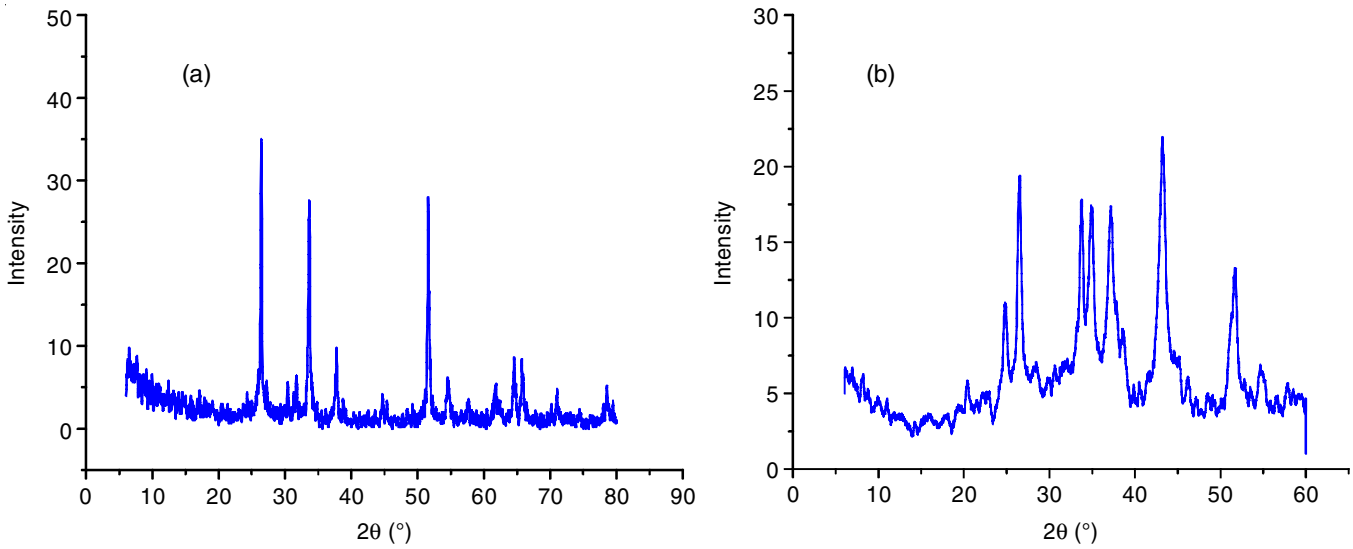

Fig. 2. XRD spectra of (a) SnS and (b) NiS/SnS nanoparticles

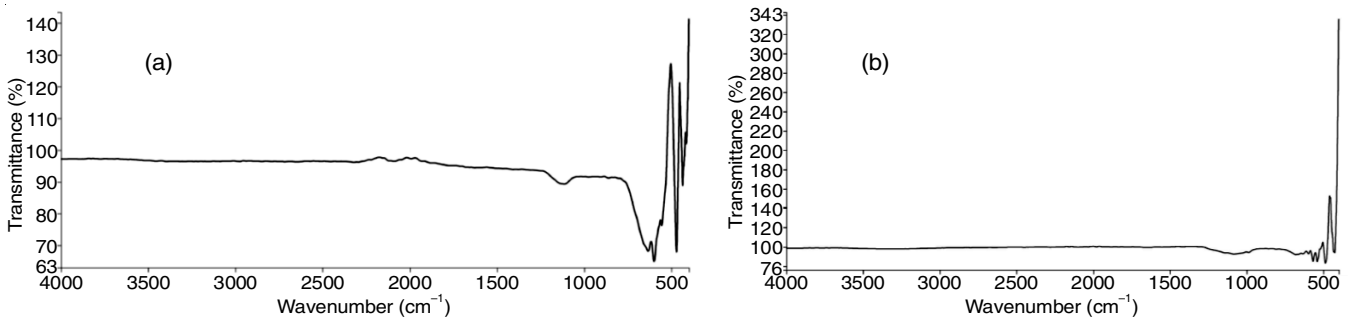

Fig. 3. FTIR spectra of (a) SnS and (b) NiS/SnS nanoparticles

changed from orthorhombic to tetragonal crystal system [28]. The XRD pattern of synthesized SnS and NiS/SnS nanoparticles are displayed in Figs. 2a-b, respectively, which exhibits sharp diffraction peaks. The XRD for SnS shows diffraction peaks at 2θ values 26.39º, 33.66º, 37.72º, 51.56º, 64.51º, 65.72º corresponding to (*hkl*) values (301), (003), (421), (442), (731) and (325), respectively. The average crystallite size was calculated using Debye-Scherrer equation and it was found to be 61.37 nm. The crystal structure parameters a = b = 11.17 Å, c = 7.984 Å and α = β = γ = 90º. Accordingly SnS belongs to tetragonal crystal system. The angle strain for synthesized SnS nanoparticles is 4.04×10^{-4}.

The XRD for NiS/SnS shows diffraction peaks at 2θ values 24.85º, 26.43º, 33.64º, 34.77º, 37.20º, 43.20º, 51.85º corresponding to (*hkl*) values (310), (301), (112), (411), (103), (422) and (204), respectively. The average crystallite size for synthesized NiS/SnS nanoparticles is 37.04 nm and angle strain is 1.08×10^{-4}. The crystal structure parameters a = b = 11.33 Å, c = 7.416 Å and α = β = γ = 90º. Accordingly NiS/SnS belongs to tetragonal crystal system.

FTIR studies: Fig. 3a shows the FTIR spectrum of SnS nanoparticles, strong and sharp bands appear in the spectrum at 2354, 1200-1000 and 615 cm^{-1}, which are due to characteristic peaks of SnS [29].

Optical absorption spectra and Tauc's plot: The optical absorption spectra of SnS and NiS/SnS nanoparticles over the range 200-800 nm exhibited maximum absorption in the UV region and there is no absorption peak in the visible region (Fig. 4). These absorption peak position reflects the band gap of the nanoparticles and the synthesized nanoparticles are photoactive under UV light radiation. The band gap of the samples were calculated from Tauc's plot found to be 2.9 eV for SnS and 2.7 eV for NiS/SnS nanoparticles as shown in Fig. 5a-b.

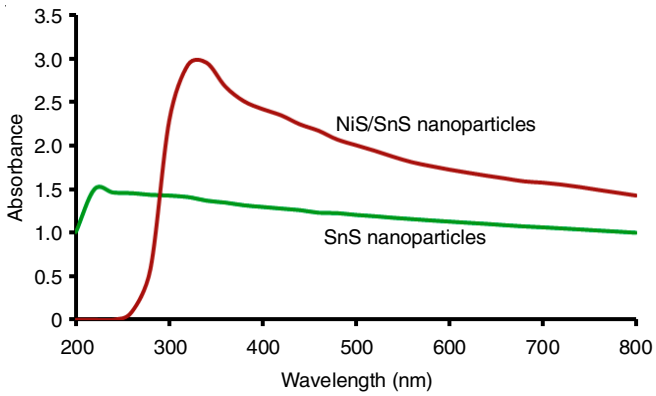

Fig. 4. Optical absorption spectra of SnS and NiS/SnS nanoparticles

SEM-EDX studies: The surface morphology of SnS and NiS/SnS nanoparticles were investigated by FE-SEM analysis as shown in Fig. 6a-b. The SEM observation revealed that the

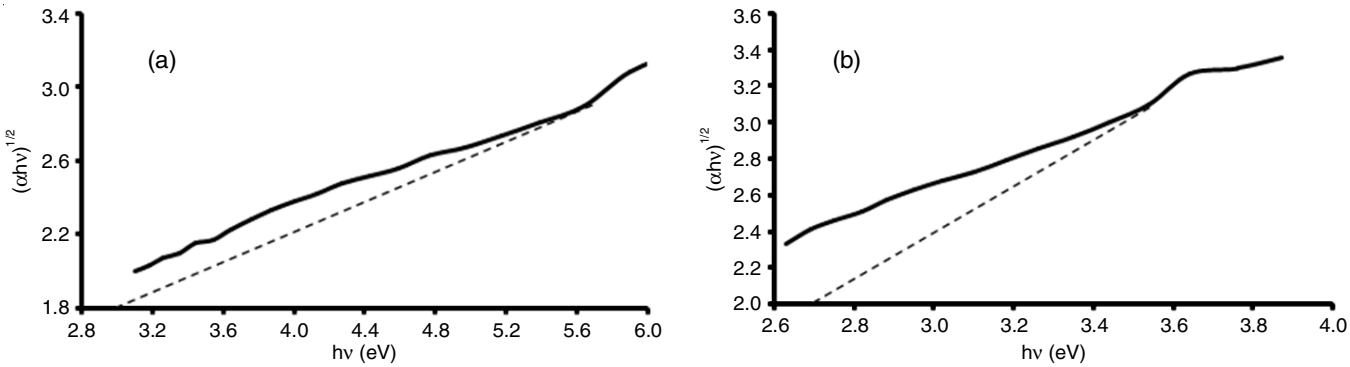

Fig. 5. Tauc's plot of (a) SnS and (b) NiS/SnS nanoparticles

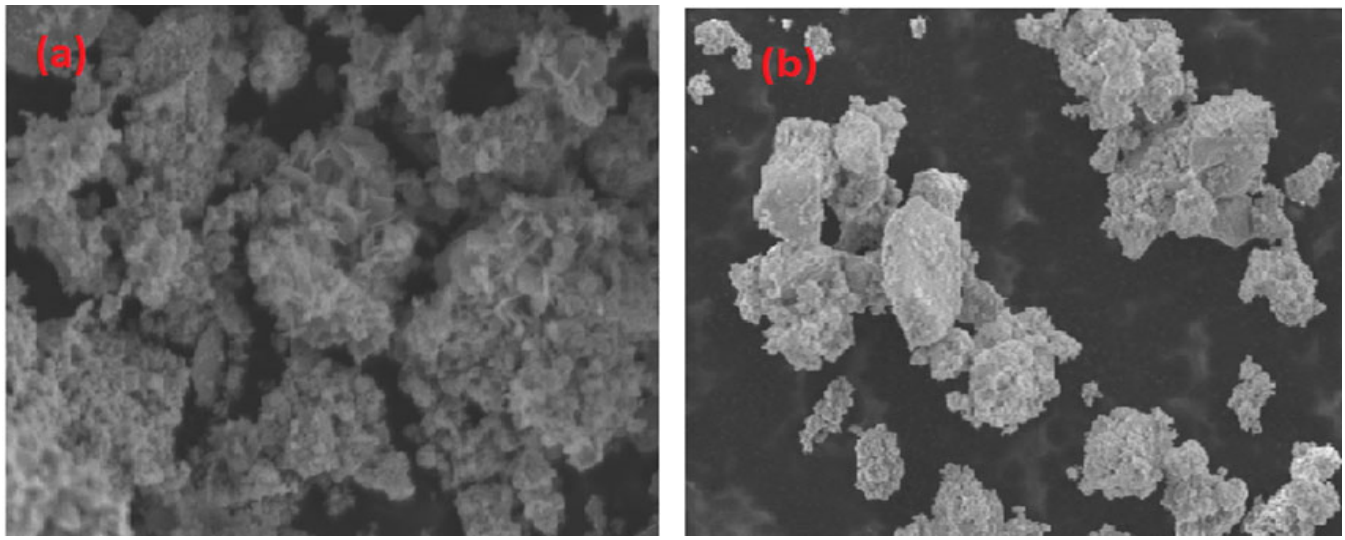

Fig. 6. FE-SEM image of (a) SnS (b) NiS/SnS nanoparticles

samples consists of aggregates of particles with cluster like structure. The elemental analysis of SnS and NiS/SnS was carried out using EDAX to confirm the presence of constituent elements (Fig. 7a-b). The synthesized nanoparticles are with high degree of purity.

Photocatalytic degradation of Indigo carmine dye and COD measurements

Effect of catalyst loading: Table-1 (for SnS) and Table-2 (for NiS/SnS) shows the rate constant of degradation with respect to different concentration of catalyst. Many studies [30,31] have indicated that the photocatalytic rate initially increases with catalyst loading and then decreases at higher values because of light scattering and screening effects. In this study, a high efficiency at a mere low concentration was achieved at 0.02 g of catalyst for both SnS and NiS/SnS nanoparticles.

Effect of concentration of dye: To ensure the optimum dye concentration, degradation is carried out with different concentration of Indigo carmine dye with constant weight of catalyst (Tables 1 and 2). As the optimum concentration of

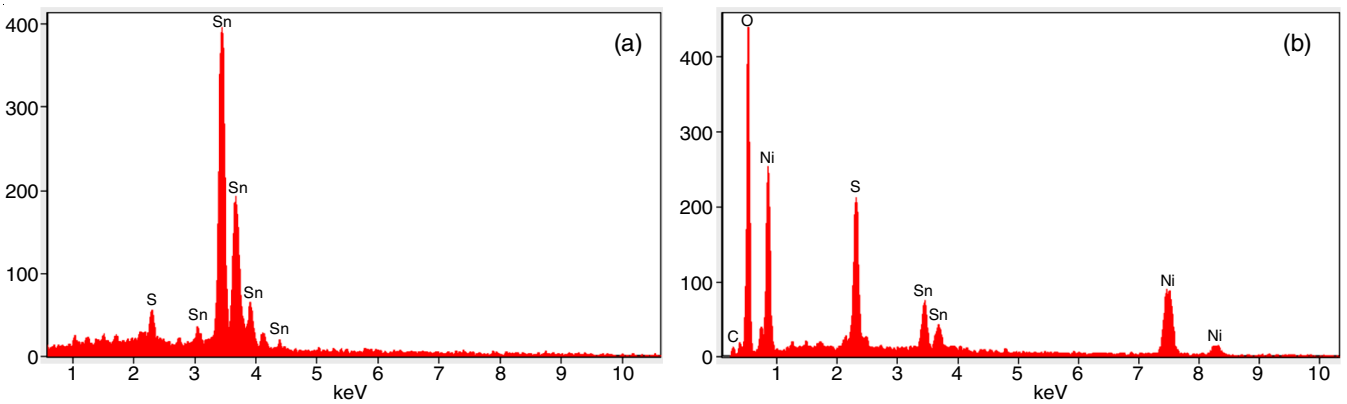

Fig. 7. Energy dispersive X-ray analysis of (a) SnS and (b) NiS/SnS nanoparticles

TABLE-1
EFFECT OF DIFFERENT VARIABLES ON THE RATE OF PHOTODEGRADATION OF INDIGO CARMINE DYE BY SnS NANOPARTICLES

Variation	Amount of catalyst/dye	k s^{-1}	Time taken for complete degradation (min)	COD values (mg/mL)		Degradation efficiency (%)
				Before degradation	After degradation	
Amount of catalyst	0.02 g	7.67×10^{-5}	80	352	16	95.45
	0.04 g	5.56×10^{-5}	120	352	16	95.45
	0.06 g	4.79×10^{-5}	140	352	32	90.90
Concentration of dye	1×10^{-5}	17.99×10^{-5}	40	304	48	84.21
	2×10^{-5}	7.67×10^{-5}	80	352	16	95.45
	3×10^{-5}	6.07×10^{-5}	210	360	64	82.22
pH 4.0	2×10^{-5}	1.74×10^{-5}	200	352	96	72.72
6.0	2×10^{-5}	3.64×10^{-5}	180	352	80	77.72
8.0	2×10^{-5}	6.52×10^{-5}	140	352	32	90.90
10.0	2×10^{-5}	11.51×10^{-5}	80	352	16	95.45
Re-use of catalyst	2×10^{-5}	6.71×10^{-5}	120	352	112	68.18

TABLE-2
EFFECT OF DIFFERENT VARIABLES ON THE RATE OF PHOTODEGRADATION OF INDIGO CARMINE DYE BY NiS/SnS NANOPARTICLES

Variation	Amount of catalyst/dye	k s^{-1}	Time taken for complete degradation (min)	COD values (mg/mL)		Degradation efficiency (%)
				Before degradation	After degradation	
Amount of catalyst	0.02 g	8.31×10^{-5}	60	352	16	95.45
	0.04 g	7.03×10^{-5}	80	352	16	95.45
	0.06 g	6.71×10^{-5}	90	352	64	81.81
Concentration of dye	1×10^{-5}	20.56×10^{-5}	40	304	32	89.47
	2×10^{-5}	8.31×10^{-5}	60	352	16	95.45
	3×10^{-5}	4.79×10^{-5}	80	360	80	77.77
pH 4.0	2×10^{-5}	5.51×10^{-5}	160	352	96	72.72
6.0	2×10^{-5}	6.71×10^{-5}	120	352	32	90.90
8.0	2×10^{-5}	23.03×10^{-5}	80	352	16	95.45
10.0	2×10^{-5}	33.58×10^{-5}	60	352	48	86.36
Re-use of catalyst	2×10^{-5}	3.72×10^{-5}	100	352	128	63.63

catalyst for SnS is 0.02g, keeping this as standard the same amount of NiS/SnS is taken for comparision for further work. As the initial concentration of dye increases degradation efficiency decreases. The reason is attributed to that more dye molecules are adsorbed on to the catalyst surface, but the adsorbed dye molecules are not degraded immediately because of the intensity of light and the amount of catalyst is constant and also the light penetration is less [30].

Effect of pH: In present work, the pH of the solution was adjusted by adding 0.01 M HCl solution and 0.01 M NaOH solution. The effect of pH was studied at pH 4, pH 6, pH 8 and pH 10 keeping all other experimental conditions constant. It can be suggested that the influence of pH on photodegradation is due to the amount of dye adsorbed on nanoparticles. It was observed that the rate of photocatalytic degradation of Indigo carmine dye increases with increase in pH up to 10 (Tables 1 and 2). This observation can be explained on the basis that as the pH of the solution increases, more OH^- ions are available. These OH^- ions will generate more. OH radicals by combining with the positive holes of the semiconductor [32]. These hydroxyl radicals are responsible for the degradation of the dye.

Reusability and regeneration of catalyst: To examine the repeatability, the photocatalyst was thoroughly washed with double distilled water, dried and reused for photodegradation by taking fresh sample of dye solution. The reuse sample has shown almost same degradation efficiency compared to the fresh samples (Fig. 8). Reuse cycles might cause aggregation of photocatalyst and the decrease in the specific surface area and the losses of catalyst [33].

Antibacterial activity: Fig. 9 shows plates to which a bacterial suspension (approximately 10^6 CFU/mL) was applied. The bacteria were grown to form a confluent lawn; the growth inhibition could be measured as the expansion of the clear zones surrounding the disc on the petri dish. The nanoparticles inhibited bacterial growth by the clear inhibition zone (concentration of 10 µg/mL). The presence of nanoparticles at certain level inhibited bacterial growth. The diameter of inhibition zones (in mm) around the nanoparticles against test strain are shown in Table-3.

Conclusion

The simple and eco-friendly electrochemical procedure has been employed to synthesize SnS and NiS/SnS semicon-

TABLE-3
ANTIBACTERIAL EFFECT OF NANOPARTICLES BY ZONE OF INHIBITION (mm) AGAINST TEST STRAINS

Bacteria	SnS	NiS/SnS	Gentamicin
Staphylococcus aureus MTCC 7443	21	19	32
Escherichia coli MTCC 40	21	12	33

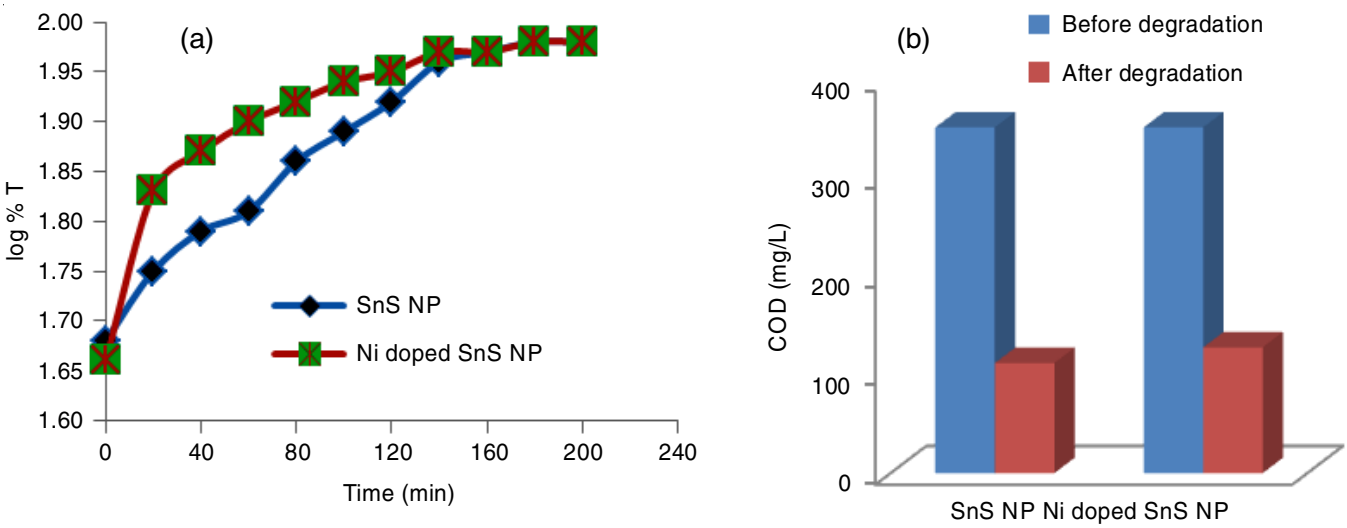

Fig. 8. Plot of log % T *vs.* time for reuse of the catalyst (a) and the effect of COD upon degradation (b) for SnS and NiS/SnS nanoparticles

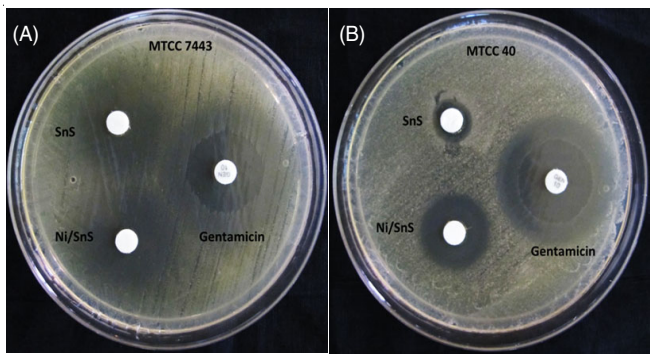

Fig. 9. Appearances of inhibitory zones with (A) *Staphylococcus aureus* and (B) *Escherichia coli* bacteria

ductor nano-photocatalysts for photocatalysis and antibacterial activity applications. The synthesized nanoparticles showed very good photocatalytic activity with respect to degradation of Indigo carmine dye under UV light radiation. The higher catalytic efficiency was achieved at low concentration of 0.02 g of catalyst. The catalytic efficiency was measured by chemical oxygen demand (COD) method. The antibacterial susceptibility of the synthesized nanoparticles evidence for its effect on biological systems.

ACKNOWLEDGEMENTS

This research work was funded by SERB-DST, UGC-BSR New Delhi, and supported by the University of Mysore. The authors greatly acknowledge UPE, CPEPA and DST-PURSE projects, Vijnana Bhavan, University of Mysore, Mysuru for providing necessary instrumentation facilities.

CONFLICT OF INTEREST

The authors declare that there is no conflict of interests regarding the publication of this article.

REFERENCES

1. V. Mlinar, *J. Mater. Chem.*, **22**, 1724 (2012); https://doi.org/10.1039/C1JM12827B
2. Z. Wang, S. Qu, X. Zeng, J. Liu, C. Zhang, F. Tan, L. Jin and Z. Wang, *J. Alloys Compd.*, **482**, 203 (2009); https://doi.org/10.1016/j.jallcom.2009.03.158
3. K.T. Reddy, N.K. Reddy and R.W. Miles, *Sol. Energy Mater. Sol. Cells*, **90**, 3041 (2006); https://doi.org/10.1016/j.solmat.2006.06.012
4. P. Tang, H. Chen, F. Cao, G. Pan, K. Wang, M. Xu and Y. Tong, *Mater. Lett.*, **65**, 450 (2011); https://doi.org/10.1016/j.matlet.2010.10.055
5. N. Koteeswara Reddy, Y.B. Hahn, M. Devika, H.R. Sumana and K.R. Gunasekhar, *J. Appl. Phys.*, **101**, 093522 (2007); https://doi.org/10.1063/1.2729450
6. P.M. Nikolic and D.M. Todorovic, *J. Phys. C Solid State Phys.*, **20**, 39 (1987); https://doi.org/10.1088/0022-3719/20/1/008
7. A.M. Tripathi and S. Mitra, *RSC Adv.*, **5**, 23671 (2015); https://doi.org/10.1039/C5RA00226E
8. S.H. Chaki, M.D. Chaudhary and M.P. Deshpande, *Adv. Nat. Sci.: Nanosci. Nanotechnol.*, **5**, 045010 (2014); https://doi.org/10.1088/2043-6262/5/4/045010
9. A. Tanusevski and D. Poelman, *Sol. Energy Mater. Sol. Cells*, **80**, 297 (2003); https://doi.org/10.1016/j.solmat.2003.06.002
10. H. Zhu, D. Yang and H. Zhang, *Mater. Lett.*, **60**, 2686 (2006); https://doi.org/10.1016/j.matlet.2006.01.065
11. W. Cai, J. Hu, Y. Zhao, H. Yang, J. Wang and W. Xiang, *Adv. Powder Technol.*, **23**, 850 (2012); https://doi.org/10.1016/j.apt.2011.12.001
12. S.S. Hegde, A.G. Kunjomana, K. Ramesh, K.A. Chandrasekharan and M. Prashantha, *Int. J. Soft Comput.*, **1**, 38 (2011).
13. M.M. El-Nahass, H.M. Zeyada, M.S. Aziz and N.A. El-Ghamaz, *Opt. Mater.*, **20**, 159 (2002); https://doi.org/10.1016/S0925-3467(02)00030-7
14. Y. Guo, W. Shi, Y. Zhang, L. Wang and G. Wei, SPIE Conference Proceedings, 69841 (2008).
15. R. Mariappan, T. Mahalingam and V. Ponnuswamy, *Optik*, **122**, 2216 (2011); https://doi.org/10.1016/j.ijleo.2011.01.015
16. S.M. Ahmed, L.A. Latif and A.K. Salim, *J. Basrah Res.*, **37**, 15 (2011).
17. Y. Ge, Y. Guo, W. Shi, Y. Qiu and G. Wei, *J. Shanghai Univ.*, **11**, 403 (2007); https://doi.org/10.1007/s11741-007-0417-1
18. E.I. Guner, F. Gode, C. Ulutas, F. Kirmizigul, G. Altindemir and C. Gumus, *Chalcogenide Lett.*, **7**, 685 (2010).
19. K. Hartman, J.L. Johnson, M.I. Bertoni, D. Recht, M.J. Aziz, M.A. Scarpulla and T. Buonassisi, *Thin Solid Films*, **519**, 7421 (2011); https://doi.org/10.1016/j.tsf.2010.12.186

20. A. Stavrinadis, J.M. Smith, C.A. Cattley, A.G. Cook, P.S. Grant and A.A.R. Watt, *Nanotechnology*, **21**, 185202 (2010); https://doi.org/10.1088/0957-4484/21/18/185202
21. Y. Li, J.P. Tu, H.M. Wu, Y.F. Yuan and D.Q. Shi, *Mater. Sci. Eng. B*, **128**, 75 (2006); https://doi.org/10.1016/j.mseb.2005.11.017
22. R.W. Miles, O.E. Ogah, G. Zoppi and I. Forbes, *Thin Solid Films*, **517**, 4702 (2009); https://doi.org/10.1016/j.tsf.2009.03.003
23. Y. Xu, N. Al-Salim, C.W. Bumby and R.D. Tilley, *J. Am. Chem. Soc.*, **131**, 15990 (2009); https://doi.org/10.1021/ja906804f
24. C. Gao, H. Shen and L. Sun, *Appl. Surf. Sci.*, **257**, 6750 (2011); https://doi.org/10.1016/j.apsusc.2011.02.116
25. O. Vázquez-Cuchillo, R. Gómez, A. Cruz-López, L.M. Torres-Martínez, R. Zanella, F.J.A. Sandoval and K. Del Ángel-Sánchez, *J. Photochem. Photobiol. Chem.*, **266**, 6 (2013); https://doi.org/10.1016/j.jphotochem.2013.05.007
26. X. Yan, R. Bao, S. Yu, Q. Li and Q. Jing, *Russian J. Phys. Chem.*, **86**, 1479 (2012); https://doi.org/10.1134/S0036024412070333
27. A.W. Bauer, W.M.M. Kirby, J.C. Sherris and M. Turck, *Am. J. Clin. Pathol.*, **45(4_ts)**, 493 (1966); https://doi.org/10.1093/ajcp/45.4_ts.493
28. N.K. Reddy, *ECS J. Solid State Sci. Technol.*, **2**, 259 (2013); https://doi.org/10.1149/2.006306jss
29. J. Henry, K. Mohanraj, S. Kannan, S. Barathan and G. Sivakumar, *J. Exp. Nanosci.*, **10**, 78 (2015); https://doi.org/10.1080/17458080.2013.788226
30. A.K. Subramani, K. Byrappa, S. Ananda, K.M. Lokanatha Rai, C. Ranganathaiah and M. Yoshimura, *Bull. Mater. Sci.*, **30**, 37 (2007); https://doi.org/10.1007/s12034-007-0007-8
31. H. Li, W. Hong, Y. Cui, Q. Jia and S. Fan, *J. Mol. Catal. Chem.*, **378**, 164 (2013); https://doi.org/10.1016/j.molcata.2013.06.012
32. B. Kaboudin, F. Kazemi, A. Ghaderian, E. Navidi and Z. Zand, *J. Sulphur Chem.*, **5**, 279 (2013); https://doi.org/10.1080/17415993.2013.863316
33. W. Sun, J. Li, G. Mele, Z. Zhang and F. Zhang, *J. Mol. Catal. Chem.*, **366**, 84 (2013); https://doi.org/10.1016/j.molcata.2012.09.010